

Ice particle habits in stratiform clouds

By A. KOROLEV^{1*}, G. A. ISAAC¹ and J. HALLETT²

¹*Meteorological Service of Canada, Toronto, ON, Canada*

²*Desert Research Institute, Reno, NV, USA*

SUMMARY

Ice crystals in clouds in the atmosphere have shapes, which relate to their density, terminal fall velocity, growth rate and radiative properties. In calculations for climate change predictions, forecasting of precipitation and remote sensing retrievals, idealized crystal shapes such as columns, needles, plates and dendrites are often assumed. The objective of this work is to study the frequency of occurrence of different habits of ice particles in natural clouds from aircraft observations. Images of cloud particles were measured by a PMS Optical Array Probe-2DC (OAP-2DC) at 25 μm resolution installed on National Research Council (NRC) Convair-580. The processing of particle images was conducted with a newly developed algorithm for pattern recognition. Data were collected during four field projects in the Canadian and US Arctic over the North Atlantic near Newfoundland, and over the Great Lakes. Approximately 5×10^6 images of cloud particles having a size larger 125 μm were analyzed. The cloud particles were classified into four categories: spheres, irregulars, needles/columns and dendrites. The habit classification of particles was done for three different size ranges: $>125\mu\text{m}$; $>250\mu\text{m}$; and $>500\mu\text{m}$. The frequency of occurrence of different habits was found for each five degree temperature interval in the range $-45^\circ\text{C} < T < 0^\circ\text{C}$. It was concluded that the majority of ice particles in natural clouds were of irregular shape. The frequency of occurrence of irregular ice decreases with increasing particle size. On average, the concentration of particles larger than 125 μm was approximately constant down to -35°C , whereas the concentration of particles larger than 500 μm decreased at temperatures below -15°C . Since the data were collected in different climatic zones within many cloud types and covered a significant cloud path length (3.6×10^4 km), the conclusions are applicable to most stratiform clouds containing ice.

KEYWORDS: Ice particle habits Ice particle concentration

1. INTRODUCTION.

A knowledge of cloud ice particle habits is of great importance for theoretical and applied cloud physics. The shape of an ice particle defines its scattering properties, its growth rate, and its terminal fall velocity. The scattering properties of cloud ice particles may significantly affect the climate and radiation balance of the whole Earth (Liou and Takano 1994; Zhang et al. 1999). Scattering properties of ice particles are also important for satellite retrievals and remote sensing (Matrosov et al. 1996). The ice particle shape affects the rate of growth through vapor deposition and riming (Mason 1994). These mechanisms define the rate of precipitation growth, which can be important for forecasting models. The terminal fall velocity influences the lifetime of ice clouds with a possible feedback on the effect of clouds on the radiation budget of the Earth.

Casual observation shows that snow particles falling from the sky appear in a great variety of shapes. The first known classification of snow particles goes back to Descartes (1902) in 1637 who classified snow habits in 10 categories. After microphotography became available at the end of last century, the number of documented forms of snow particles were counted by hundreds and thousands (Bentley 1902). Almost every researcher has developed their own

Corresponding author: Alexei Korolev, Meteorological Service of Canada, 4905 Dufferin St., Downsview, Ontario, M3H 5T4, Canada. e-mail: Alexei.Korolev@ec.gc.ca

classification of snow habits. Later the great variety of snow forms were grouped using different indicators in a smaller number of categories. Thus, Nakaya (1954) used 41 categories for the classification of ice particles. Zamorsky (1955) suggested 72 categories of ice particles; Magono and Lee (1966) classified natural snow crystals in 80 categories. From the crystallographic point of view, the basic shape of an ice crystal is a six fold symmetric (hexagonal) prism with two basal planes and six prism planes (e.g. Hobbs 1974). Early laboratory experiments revealed that the rate of propagation of the basal faces (along the *c*-axis), relative to that of prism faces (along the *a*-axis) varies with temperature and supersaturation in a characteristic manner (e.g. Nakaya 1954; Kobayashi 1957; Hallett and Mason 1958; Rottner and Vali 1974). Observation of ice particle shapes in natural conditions collected by different authors have been summarized by Magono and Lee (1966) in the well known Magono-Lee diagram.

Although the classification of ice particles does not provide any information about the frequency of occurrence of ice particle habits, it may considerably bias a general impression. Thus, the numerous pictures of beautiful pristine dendrites and plates by Bentley and Humphreys (1931), probably taken in part for aesthetic reasons, has lead to publications such as the Encyclopedia Britannica (1947), implying that most snow crystals had similar shapes. Existing numerical models for weather forecast or climate changes approximate snow particle shape by hexagonal plates or columns. On the other hand simple surface observations of snow particles show that some habit categories occur more frequently than others and many particles are of irregular shape.

There are only a few studies of the climatology of snow habits. Zamorsky (1955 p. 264-269) during the winter of 1945/46, studied the frequency of occurrence of 48 different habit categories of snow particles. From his observation it follows that monocrystalline ice particles as plates, columns and stellar crystals were observed in 2.2%, 9.0% and 0.4% of cases, respectively. The rest of the snow particles were described as having polycrystalline habit. These measurements were conducted at ground level and the temperature range is unknown. Isaac (1991) studied the percentage of different ice particle habits in Canadian Atlantic storms and found a maximum occurrence of needles and sector plates at -3°C and -16°C , respectively. However, in this study, 80% of the time images were observed which could not be classified.

The aircraft observation of ice particle habits conducted in Arctic clouds with the help of a newly developed Cloud Particle Imager (CPI) probe (Lawson 1997) showed that the majority of ice particles were faceted composite crystals with different crystallographic orientations growing in different directions (Korolev et al. 1999). In many cases the ice particles consisted of faceted and non-faceted parts. The frequency of occurrence of faceted monocrystalline (pristine) ice particles was found to be only 3%. The understanding of mechanisms that lead to the formation of irregular shape polycrystalline particles has great importance for cloud physics and its applications.

Before the 70's, the main instruments for aircraft measurements of the habits of cloud ice particles were different types of impactors. Though the impactors provide a large dynamic range of particle sizing (from few micrometers to few millimeters), one of the main problems in using this technique is that ice particles break during the impact with the impactor surface. This makes it difficult to recognize the shape of particles $> 500\mu\text{m}$ (Hallett 1976). The processing of data obtained using an impactor technique is not a simple task and is time consuming. In the mid 70's Particle Measuring System Inc. (PMS) developed Optical Array Probes for aircraft measurements of two-dimensional shadow images of cloud particles (Knollenberg 1981). Since that time, these instruments have become one of the major instruments for studies of cloud microstructure. Paradoxically, although they were installed on a majority of cloud research

aircraft and were in use for almost thirty years, there are only a few studies analyzing the frequency of occurrence of ice habits. The data were mainly used for calculation of particle size distribution, whereas the information on the shape of particles remained mostly unprocessed. This was probably due in part to the complexity of 2D-image processing and the lack of image recognition software and in part to the complexity of the images themselves.

The current work presents a study of ice particle habits based on PMS OAP-2DC measurements. The images were classified into four categories: irregulars, dendrites/aggregates, columns/needles and circular images, implying mostly a spherical shape. The OAP 2D-data were processed with an algorithm originally developed for automated particle pattern recognition. This algorithm is based on determining the fraction of ice particles having a certain habit from the distribution of geometrical ratios calculated for an ensemble of images. The data were collected during four different field projects in the Arctic and in mid-latitude regions. The results of this work show that the majority of ice particles in natural, mainly stratiform, clouds have an irregular shape. Since the data were collected in different climatic zones and covered a significant cloud path length, the conclusions of this work may be generalized to all stratiform clouds.

2. INSTRUMENTATION

The cloud particle images were measured by a PMS Optical Array Probe OAP-2DC installed on the NRC Convair-580. The principle of particle imaging (Knollenberg 1981) is based on obtaining measurements of particle shadow with the help of a linear array of photodetectors. The optical system, using a He-Ne laser, produces an intense illumination such that the particle images are dark shadows on a bright background. The particle shadows are projected on a linear array of photodiode elements. This detector array is used as a measuring grid to image the shadows of particles. When a particle traverses the laser beam, its imaged shadow covers a number of optical array elements. The element is considered to be covered if the loss of light is at least 50%. The photodiode produces image slices with the rate synchronized with true air speed to get the same resolution along the flight direction (X-axis) and the direction of orientation of the photodiode array (Y-axis). The output of the probe is binary (black and white) discrete images, as shown in Fig. 1. The probe used in this study has a photodiode array with 32 elements, with a resolution set at 25 μ m.

Fogging of the optics during fast descents, ice buildup on the instruments, and droplet shedding may have a significant effect on the measurements. The data were carefully examined for indications of fogging, icing, and shedding. All these cases were excluded from data analysis

3. ALGORITHM AND DATA PROCESSING

(a) Overview of existing algorithm

There are several different algorithms developed for OAP-2D image recognition. Heymsfield and Parrish (1979a) used a simple relationship between the particle image size and the ratio of the image area to that of an equivalent diameter sphere to derive the particle habit. Rahman et al. (1981) used different geometrical parameters applied to artificial idealized images of ice particles and maximum likelihood Bayes family classes (Tou and Gonzales 1974). Duroure (1982) performed a radial analysis of particle image. A Fourier transform was then used to extract shape discrimination from the image parameters of the analyzed data set. Hunter et al. (1984) used a specially constructed vector consisting of FFT radial frequency, size parameter and sums of occulted pixels in image slices. Holroyd (1987) used a value of the dimensionless geometrical ratio PD_{max}/S , where P is particle image perimeter; S is the area of the image; D_{max} is

maximum dimension of the image, to classify ice particle images. Moss and Johnson (1994) used a pattern recognition technique similar to the one described by Duroure (1982) but with different criteria for categorizing cloud particles. Duroure et al. (1994) used a relation between S and P of individual images to characterize habits of the population of particles. Garbrick et al. (1995) developed a method based on a neural network technique. Fouilloux et al. (1997) developed a technique for statistical analysis of habits of small spheres and columns based on characteristic position of triggered pixels in its images.

(b) Basics of the algorithm

The present algorithm classifies particle habits by analyzing dimensionless ratios of simple geometrical measures such as the X- and Y-dimensions, perimeter and image area (Korolev and Sussman 2000). The key to this method lies in considering these ratios for an ensemble of images. It is assumed that each habit category has a unique distribution of ratios. For an ensemble of images presented by a mixture of different habits, the distribution of a particular ratio will be a superposition of distributions of ratios of individual habits. If these distributions are known, than the fraction of each habit for an ensemble of 2D-images can be found as the solution of an inverse problem.

In the present analysis, the following measurable parameters of 2D-images were used (Fig. 1): N_x the number of pixels in the X-direction (perpendicular to the photodiode array, i.e. along the flight direction), N_y the number of pixels in the Y-direction (parallel to the photodiode array), N_{total} the total number of shadowed pixels, N_{edge} the total number of triggered edge pixels, N_{edge1} , N_{edge2} the number of triggered edge pixels on each side of the particle image, and N_P the number of perimeter pixels. The measurable parameters can be converted into the corresponding geometrical parameters as follows: $D_x = \delta N_x$ the particle image X-size; $D_y = \delta N_y$ the particle image Y-size; $S = \delta^2 N_{total}$ the particle shadow image area; $P = \delta N_P$ the particle image perimeter. Here $\delta = 25\mu\text{m}$ is the probe pixel resolution.

(c) Habit categories

The present algorithm classifies 2D-images into four habit categories: "spheres", "irregulars", "needles" and "dendrites" (Fig. 2).

The class "spheres" (Fig. 2a) includes particles with circular images. Such particles could be liquid drops or quasi-spherical ice particles like graupel or frozen drops. In some cases flat solid particles, like hexagonal plates, may also give quasi-circular images. However, as it will be discussed below, the effect of plates on the frequency of occurrence of spherical particles is small.

The category "needles" (Fig. 2c) includes images having elongated quasi-rectangular projection with aspect ratio $C/A > 3$, here C is the length along the c -axis, and A is the diameter in the a -axis direction. Such projections in the majority of cases are produced by needles or columns. Rosettes with 3 to 5 bullets also fall in the category "needles". Planar crystals like plates or dendrites may also give a needle-like projection viewed edge on, although the effect of such particles on the statistics of habit occurrence in this study is negligible (see Section 6).

The class "dendrites" (Fig. 2d) includes dendrites, stellar crystals, or aggregates of dendrites.

The category "irregulars" (Fig. 2b) includes particles having an irregular or random shape, which does not fall into any of the above three categories. Polycrystalline ice particles such as combination of plates or columns, heavily rimed particles, graupel, and other forms that

do not display features “needles”, ”dendrites” or “spheres” would fall into the category “irregulars”.

Different authors used different numbers and types of habit categories in their automated classifiers of OAP images. Rahman et al. (1981) recognized seven classes of particle habits: drop, graupel, stellar crystal, spatial dendrite, column, capped column, and plate. Duroure (1982) classified particles in eight habit categories: drop, graupel, stellar crystal, spatial dendrite and aggregate, plate, and needle and column. Hunter et al. (1984) used six classes to categorize OAP-2D images: dendrite, needle, column or bullet, plate or sphere, streaker, and miscellaneous. Holroyd (1987) and Garbric et al. (1995) categorized particle habits in eight classes: sphere, hexagonal, graupel, linear, oriented, dendrite, aggregate, and irregular. Moss and Johnson (1994) distinguished nine categories for habit recognition: droplet, large droplet, small droplet, small ice, graupel, stellar, symmetric, column, and aggregate.

Some authors claim to be able to recognize hexagonal plates starting from images having 3 to 5 pixels in size. However, hexagonal plates would display a hexagonal structure only with images having at least 12 to 14 pixels in “diameter” (Korolev and Sussman 2000). Plates with smaller sizes would fall into another category other than “plate”. Therefore, the fraction of plates calculated for an ensemble of particles using the above classifiers would be *a priori* biased. For this reason the category of plates was not included into our analysis. The current four categories cover the major habits of ice particles in troposphere clouds. Because of the poor size resolution (25 μm), the small field of view (32 pixels in width), and the low gray level resolution (black and white), habit recognition analysis is significantly limited. The level of riming, or a judgement about whether crystals are pristine (single crystals with well defined facets), cannot be made. However, statistics on the occurrence of major ice habit categories are valuable for remote sensing retrievals, parameterization of GCM models, and understanding ice formation in the atmosphere.

(d) Image groups

The classification begins with a break down of 2D-images into four groups: "tiny", "rejected partials", "complete", and "accepted partials".

(a). The “tiny” images were defined as images that triggered less than N_x^* or N_y^* pixels. In the context of this work the threshold values were $N_x^* = N_y^* = 5, 10$ or 20 pixels. These numbers correspond to actual particle sizes $125\mu\text{m}$; $250\mu\text{m}$; $500\mu\text{m}$, respectively. The images having sizes less than $125\mu\text{m}$ (5pixels) were considered too small for image recognition analysis. The use of different threshold sizes for N_x^* and N_y^* make it possible to analyze the dependence on particle size of the frequency of occurrence of particle habits.

(b). The group of "rejected partials" consists of particles where the largest part of the image is assumed to be out of the image frame. Such images were defined as $N_{total} \leq 180$, and $N_{edge} \geq 4$ and $N_y < 32$. Preliminary analysis showed that the recognition of such images gives poor results. Fig. 3b shows an example of "rejected partials". Images containing empty slices inside the shadowed zone along the Y-axis (flight direction) were also rejected (Fig. 3c). Such images usually occur in the case of fogging and in some special cases of probe malfunctions.

(c). The third group, "complete" images, includes the images with the number of triggered pixels $N_x > N_x^*$ or $N_y > N_y^*$ with the total number of edge pixels $N_{edge} < 4$.

(d). The "accepted partial" images were defined as 2D-images with $N_{total} > 180$ pixels and $N_{edge} \geq 4$ or $N_y = 32$, which is maximum number of pixels in the Y-direction.

The next step of the algorithm is the calculation of the distribution of geometrical ratios for an ensemble of 2D-images. Eighteen different ratios were considered for both "complete" and "partial" images. Each ratio was tested on special samples of images of natural cloud particles to provide the best habit recognition.

(e) "Complete" images

For "complete" images the ratio

$$R_1 = \frac{\pi(N_x^2 + N_y^2)}{8N_{total}} = \frac{\pi(D_x^2 + D_y^2)}{8S} \quad (1)$$

was found to have the most unique features to characterize each category of habits. Perfect spheres give circular images, $R_1=1$. Due to imperfections of images caused by discretisation (Korolev et al. 1998) or the probe electronics, the value of R_1 for real spherical particles may be different from 1. Therefore the images from an ensemble of spherical particles return a narrow frequency distribution of R_1 centered around $R_1=1$. Needles and columns are defined as rectangles having a length-to-width ratio (C/A) of between 3 to 8. Therefore, for needles and columns the ratio $R_1 \approx \frac{\pi C}{8A}$ ranges somehow from 1 to 3. Due to their unique shape, dendrites and irregular particles will also return a unique distribution for the ratio R_1 . Notice, that although all distributions overlap, each habit category leaves a unique distribution signature.

(f) "Partial" images

The "partial" images were classified in a different way. The classification begins by assuming that the particle image is a perfect circle. Knowing the number of triggered edge pixels on the image N_{edge1} and N_{edge2} , the perimeter of the sphere can be found as

$$P_{circ} = 2(\theta_2 - \theta_1)r \quad (2)$$

Here

$$r = \sqrt{\frac{x_1^2}{4} + \left(\frac{y_0}{2} + \frac{x_2^2 - x_1^2}{8y_0}\right)^2} \quad (2a)$$

$$\theta_1 = \arctan\left(\frac{x_1}{2z}\right) \quad (2b)$$

$$\theta_2 = \arctan\left(\frac{x_2}{2(z + y_0)}\right) \quad (2c)$$

$$z = \frac{x_1^2 - x_2^2}{8y_0} - \frac{y_0}{2} + r \quad (2d)$$

$$x_1 = \delta N_{edge1}; \quad x_2 = \delta N_{edge2}; \quad y_0 = 32 \delta$$

The assumed circle image perimeter can then compared with the measured one, i.e.

$$R_2 = \frac{P_{meas}}{P_{circ}} \quad (3)$$

(g) Construction of a retrieval matrix

For each image category a distribution of the geometrical ratio $B_i(R)$ was calculated using a test set of images (Fig. 2), where $i=1,2,3,4$ is a conditional number corresponding to each

image category. To build a retrieval matrix, the distributions $B_i(R)$ should be converted into a discrete function $B_{ij}(R)$ such that

$$B_{ij} = \int_{R_j}^{R_{j+1}} B_i(R) dR \bigg/ \int_0^{\infty} B_i(R) dR \quad (4)$$

Then the retrieval matrix can be represented as

$$\mathbf{B} = \begin{pmatrix} B_1^* \\ B_2^* \\ B_3^* \\ B_4^* \end{pmatrix} \quad (5)$$

Here B_i^* are the vectors with the elements defined by Eq. 4.

One of the necessary conditions to get a unique solution is that the matrix \mathbf{B} must be square. Hence, the number of elements in the vector B_i^* must be equal to the number of image categories. In order to find the vector B_i^* , the geometrical ratio R should be split into intervals $[R_j, R_{j+1}]$, where $j=1,2,3,4$. The boundaries of the intervals $[R_j, R_{j+1}]$ were chosen by performing an optimizing of \mathbf{B} that minimized its condition number. The condition number is the ratio of the largest singular value of \mathbf{B} to the smallest. The conditioning number measures the sensitivity of the solution of a system of linear equations to errors in the data.

After the matrix \mathbf{B} is constructed, the fraction of images in each habit category can be found as

$$\vec{f} = \mathbf{B}^{-1} \vec{M} \quad (6)$$

where \vec{M} is a 1-by-4 vector describing the measured distribution of the geometrical ratio for an ensemble of 2D-images in the intervals $[R_j, R_{j+1}]$; \vec{f} is a vector of fractions of images belonging to the different habit categories. For example if $\vec{f}=(0.5, 0.2, 0.05, 0.25)$ then the composition of the sample would be 50% spheres, 20% irregulars, 5% needles/columns and 25% dendrites.

The final step is to sum the vectors \vec{f}_c and \vec{f}_p for "complete" and "partial" images, respectively. This is done by weighting each vector with respect to the number of "complete" (N_c) and "partial" (N_p) particles it represents.

$$\vec{f} = \frac{N_c \vec{f}_c + N_p \vec{f}_p}{N_c + N_p} \quad (7)$$

In order for this procedure to be effective, the size of the 2D-image sample should be statistically significant. If only a small number of images (less than 100) are used to calculate \vec{M} , then the errors related to Poisson statistics, may well exceed 20%. The subsequent retrieval procedure may only increase these errors. A sample size of five buffers (32x1024 pixels) usually represents 200 to 400 particles acceptable for image analysis. Therefore, five buffers are large enough to accurately describe the fractional composition of particle shapes, while at the same time being sufficiently small so as to suitably display the spatial variations of particle habits in a cloud.

(h) Accuracy of the method

Figure 4 shows the results of the image recognition analysis for a flight on 23 January 1998 during the Canadian Freezing Drizzle Experiment III (Isaac et al., 1998). The panels Fig. 4

b, c, d, and e show the fraction of irregulars, dendrites, needles and spheres, respectively, derived from the OAP-2DC data. It is seen that dendrites and needles occur in cells, where the fraction of needles and dendrites may reach up to 90%-100%. Figure 5 shows the OAP-2DC images measured in zones with a high percentage of circulars (a), irregulars (b), dendrites (c), and needles (d). A comparison of the results of habit recognition using the present algorithm, with those performed by eye, shows that for randomly chosen sets of images contained in five 2D-buffers, the error in misclassifying particle habits does not exceed 10%-15% on average.

4. FREQUENCY OF OCCURRENCE OF ICE PARTICLE HABITS

The data on ice particle habits were collected during four field campaigns: the Beaufort Arctic Storm Experiment (BASE) in September-October 1994, the Canadian Freezing Drizzle Experiment I (CFDE I) in March 1995, the Canadian Freezing Drizzle Experiment III (CFDE III) December 1997-February 1998, and FIRE.ACE in April 1998. The number of flights with the NRC Convair-580 included in the analysis, the type of air mass, and the region of the flights are indicated in Table 1. Usually the duration of the NRC Convair-580 flights was between 2 and 5 hours.

The main bulk of data were collected in stratiform clouds (*St*, *Sc*, *Ns*, *As*, *Ac*), usually associated with frontal systems. During the BASE and FIRE.ACE projects, a number of flights sampled cirrus clouds. The total flight length in cloud was 35,840 km. The temperature and altitude of measurements ranged from 0 to -45°C and from 0 to 7.5 km, respectively.

Within this study, about 3×10^7 particle images were analyzed. Most of the images were rejected as "tiny" with size less $125 \mu\text{m}$ (2.2×10^7 images) or "rejected partials" (2.3×10^6 images). About 5×10^6 images, having sizes larger than $125 \mu\text{m}$, were accepted for pattern recognition. Approximately 35% of accepted images were "partials" (section 3d). The frequency of occurrence of ice particle habits was calculated for 5-degree temperature intervals in the range 0°C to -45°C . The results of the processing are presented in Table 2 for BASE, Table 3 for CFDE I, Table 4 for CFDE III, and Table 5 for FIRE.ACE. Table 6 shows the frequency of occurrence of ice particle habits averaged over the four projects.

(a) Irregular particles

The most important finding of this study is that the fraction of irregular particles is dominant over other forms *in all temperature intervals*. On average, the fraction of irregulars in the analyzed data set is 84% for $D > 125 \mu\text{m}$, and 76% for $D > 500 \mu\text{m}$ (Table 6). There were a number of flights where 95-98% of all particles were recognized as irregulars regardless of particle size. The fraction of irregular particles with $D > 125 \mu\text{m}$ and $D > 250 \mu\text{m}$ on average gradually increases from 69% and 63%, respectively, at 0°C to 95% and 97%, respectively, at -40°C (Fig. 6a). Below -40°C , the fraction of irregulars with $D > 125 \mu\text{m}$ and $D > 250 \mu\text{m}$ decreases. For particles with $D > 500 \mu\text{m}$ the fraction of irregulars has a maximum (88%) at -25°C to -30°C and decreases below this temperature.

On average irregulars with $D > 125 \mu\text{m}$ are more common than those with $D > 500 \mu\text{m}$. This phenomenon is especially noticeable in the temperature intervals $-15^{\circ}\text{C} < T < 0^{\circ}\text{C}$ and $-45^{\circ}\text{C} < T < -30^{\circ}\text{C}$ (Fig. 6a). The diagrams in Fig. 7 clearly show the changes of the fraction of irregulars observed during FIRE.ACE from 67% for $D > 125 \mu\text{m}$ down to 34% for $D > 500 \mu\text{m}$ in the temperature interval $-10^{\circ}\text{C} < T < -5^{\circ}\text{C}$. At temperatures $-40^{\circ}\text{C} < T < -15^{\circ}\text{C}$ the fraction of irregulars does not change significantly with an increase of particle size. However, it reduces again noticeably with an increase of particle size at temperature $-40^{\circ}\text{C} < T < -45^{\circ}\text{C}$. The decrease in

the fraction of irregulars results from an increase in the fraction of dendrites at $-15^{\circ}\text{C} < T < -0^{\circ}\text{C}$ and needles at $-45^{\circ}\text{C} < T < -30^{\circ}\text{C}$ (Fig. 7).

The Magono-Lee diagram does not show irregular shaped particles in the temperature interval $-20^{\circ}\text{C} < T < -15^{\circ}\text{C}$ and $-35^{\circ}\text{C} < T < -30^{\circ}\text{C}$. However, the OAP-2DC imagery of cloud particles indicated that the fractions of irregular particles in these temperature intervals are 84% and 93%, respectively (Table 6).

(b) Dendrites

On average the fraction of dendrites at temperatures $-45^{\circ}\text{C} < T < 0^{\circ}\text{C}$ is 3% and 10% for particles with $D > 125\mu\text{m}$ and $D > 500\mu\text{m}$, respectively (Table 6). The fraction of dendrites increases with an increase of particle size at $-15^{\circ}\text{C} < T < 0^{\circ}\text{C}$ (Fig. 6b). For example during FIRE.ACE the fraction of dendrites increased from 17% to 55% when the threshold size increased from $125\mu\text{m}$ to $500\mu\text{m}$ at $-15^{\circ}\text{C} < T < -10^{\circ}\text{C}$ (Fig. 7).

The maximum frequency of occurrence of dendrites was observed in the temperature interval $-15^{\circ}\text{C} < T < -10^{\circ}\text{C}$ (Fig. 6b). This is consistent with the dendritic growth of ice particles observed in laboratory and in natural conditions (e.g. Hallett and Mason 1958; Magono and Lee 1966; Rottner and Vali 1974). However, in the majority of cases at $-15^{\circ}\text{C} < T < -10^{\circ}\text{C}$, there are no dendrites at all, and the dominant ice particle habit is irregular. This fact is not reflected in the Magono-Lee diagram. Though the Magono-Lee diagram has categories "graupel" (R3a, R3b, R3c in Magono-Lee classification) and "graupellike" (R4a, R4b, R4c), which would be interpreted as irregulars, there are a large variety of irregular ice particle shapes observed at $-15^{\circ}\text{C} < T < -10^{\circ}\text{C}$, which do not fit into these two categories. Graupel particles would also make an impact noise on the aircraft, and this was very rarely observed during the flights. It is unlikely that many of the classified irregular particles were graupel.

A significant number of dendrites were observed within the temperature interval $-10^{\circ}\text{C} < T < 0^{\circ}\text{C}$ (Tables 2-6). Thus, during FIRE.ACE the fraction of dendrites with $D > 500\mu\text{m}$ was 55% in the temperature interval $-10^{\circ}\text{C} < T < -5^{\circ}\text{C}$. These dendrites were likely formed in the upper layers at colder temperatures and then fell down to the lower warmer layers still keeping their dendritic shape. It is worth noting that the Magono-Lee diagram does not show dendrites at temperatures $-10^{\circ}\text{C} < T < 0^{\circ}\text{C}$.

The dendritic ice particles occur in isolated cells embedded in zones of irregular shape ice particles (Fig. 4c). In such cells the fraction of dendrites may reach 100%. In most cases, the ice particles in such cells are a mix of dendrites and irregulars and/or needles (Fig. 8a). The characteristic size of these cells is several kilometers, though it may range from hundreds of meters to tens of kilometers (Fig. 4c). The observation of dendrites in isolated cells leads to the conclusion that dendritic growth in clouds at temperatures $-15^{\circ}\text{C} < T < -10^{\circ}\text{C}$ occurs only in limited conditions.

Particles recognized as dendrites at temperatures below -20°C may be multiple bullet rosettes that resemble dendrites. However, the fraction of such particles often does not exceed 2% (Table 6). Such values may also be explained by errors in the shape recognition technique. The frequency of occurrence of dendrites in Arctic clouds (Tables 2,5) was found to be higher than in mid-latitude clouds (Tables 3,4).

(c) Needles and columns

On average the fraction of needles and columns is about 6% and 8% for $D > 125\mu\text{m}$ and $D > 500\mu\text{m}$, respectively (Table 6). The fraction of needles/columns increases with an increase of particle size at $-5^{\circ}\text{C} < T < 0^{\circ}\text{C}$ and $-45^{\circ}\text{C} < T < -40^{\circ}\text{C}$. For all four projects the maximum of the

fraction of needles was observed in the $-5^{\circ}\text{C} < T < 0^{\circ}\text{C}$ temperature interval (Fig. 6c). At these temperatures the percentage of needles varies between 11% and 22% for $D > 125\mu\text{m}$ and between 12% and 33% for $D > 500\mu\text{m}$, respectively (Tables 2-5). There is only a small fraction of columns at temperatures $-35^{\circ}\text{C} < T < -10^{\circ}\text{C}$.

The observation of maximum of frequency of occurrence of needles at $-5^{\circ}\text{C} < T < 0^{\circ}\text{C}$ is in agreement with observations of needle growth in laboratory studies (e.g. Hallett and Mason 1958; Magono and Lee 1966; Rottner and Vali, 1974; Keller and Hallett 1982; Alena et al 1990). Another increase in the frequency of occurrence of columns occurs at low temperatures $-45^{\circ}\text{C} < T < -40^{\circ}\text{C}$. This is consistent with an increase of occurrence of pristine ice particles, mainly columns, towards low temperature observed during FIRE.ACE in Arctic clouds (Korolev et al. 1999).

The Magono-Lee diagram shows that in the temperature interval $-35^{\circ}\text{C} < T < -30^{\circ}\text{C}$ ice particles in natural clouds should consist of columns or rosettes of bullets. The algorithm used in this study would classify these particles as “columns”. However, the OAP-2DC data showed that the fraction of columns is only 2% in this temperature interval. This indicates a big divergence between observation of ice particles in the interval $-35^{\circ}\text{C} < T < -30^{\circ}\text{C}$ in the frame of this study and the Magono-Lee diagram. This may be attributed to variations in ambient supersaturation which influence growth habit at low values (Hallett et al. 2000).

As was found for dendrites, in many cases the needles at warm temperatures ($-5^{\circ}\text{C} < T < 0^{\circ}\text{C}$) and columns at cold temperatures ($-45^{\circ}\text{C} < T < -40^{\circ}\text{C}$) occurred in cells (Fig. 4). The characteristic horizontal dimensions of these zones or cells are several kilometers. The needles in such cells are frequently mixed with irregulars (Fig. 8a,b) or more rarely mixed with dendrites (Fig. 8a).

(d) Spherical particles

On average, spherical particles represent 7% and 6% of the classified images for the size intervals $125\mu\text{m}$ and $500\mu\text{m}$, respectively (Table 6). A large number of spherical particles (from 6 to 20%) were observed in the temperature interval $-10^{\circ}\text{C} < T < 0^{\circ}\text{C}$ during CFDE I (Table 3) and CFDE III (Table 4). These particles were mainly associated with freezing drizzle events and were either liquid or frozen droplets. In contrast in Arctic clouds, the spherical particles were more or less evenly distributed within the $-40^{\circ}\text{C} < T < 0^{\circ}\text{C}$ temperature interval. This is consistent with our numerous observations of CPI images of quasi-spherical particles in cirrus and mid-level clouds in the Arctic during FIRE.ACE. It is possible that, due to a poor of resolution and digitizing problems of the OAP-2DC (Korolev et. al 1998) some irregulars were categorized as spherical particles. However, these types of errors do not exceed several percent on average and do not affect significantly the statistical results. It should be noted that hexagonal plates could also be classified as spherical particles. However as will be discussed in section 6bc, the effect of hexagonal plates or columns on the statistics of ice habit frequency is negligible.

The fraction of spherical particles gradually decreases towards low temperatures from 13% at temperature $-5^{\circ}\text{C} < T < 0^{\circ}\text{C}$ down to 0% at $-45^{\circ}\text{C} < T < -40^{\circ}\text{C}$ for $D > 125\mu\text{m}$ particles (Table 6). A similar trend is observed for $D > 500\mu\text{m}$ particles (Table 6). During CFDE III and AIRS the PMS OAP and CPI measured freezing drizzle at temperatures as cold as -20°C to -27°C , at altitudes between 5-7 km. The size of liquid drops reached $200\mu\text{m}$. Besides drizzle size drops, high resolution CPI images showed the presence of a large concentrations of ice pellets in this area. It is worth noting that the Magono-Lee diagram does not show spherical or quasi-spherical particles at temperatures below -15°C .

5. CONCENTRATION OF ICE PARTICLES

The number concentration of ice particles was estimated as

$$N = n/SL_{cloud} , \quad (8)$$

where n is total number of analyzed particles larger than 125 μm , 250 μm , or 500 μm measured over a cloud path length L_{cloud} , $S=lw$ is the sample area of the OAP-2DC, l is the depth-of-field of the sample area ($l=61\text{mm}$), $w=m\delta$ is the width of the sample area ($w=1.6\text{mm}$), $m=32$ is the number of photodiodes in the photodiode array, and $\delta=25\mu\text{m}$ is the resolution of the probe. For particles larger than 125 μm , the depth-of-field of the OAP-2DC is constant and independent of the particle size (e.g. Korolev et al. 1998). However, the width of the sample area is a function of particle size (Heymsfield and Parrish 1979b). For “complete” images, which do not touch the edge elements, the actual width is less than that estimated as w , and for partial images it is larger than w . Therefore, the effective width of the sample area w_{eff} depends on the particle size distribution. Since in the majority of cases the particle size distribution is a monotonically decreasing function with size, the effect of smaller particles on w is larger than that of large ones. Hence, $w_{eff}<w$, and the particle concentration calculated using Eq. (8) gives an estimated upper limit of the particle number concentration.

The distance L_{cloud} refers to ice, mixed and liquid clouds. A cloud was defined as an area where water content derived from FSSP measurements in size range 5-95 μm was no less than 0.0008 gm^{-3} . A special analysis showed that such definition covers (a) all liquid clouds; (b) all mixed clouds; (c) ice clouds where OAP-2DC is triggering. The advantage of this definition is that it is not sensitive to aerosol, and at the same time it includes liquid clouds “invisible” to the OAP-2DC.

In order to avoid misinterpretation, it is worth noting that the particle concentration estimated from Eq. 8 is a result of averaging over the distance L_{cloud} , the value of which is of the order of magnitude 10^1 to 10^3km (Tables 1-6). The scale of L_{cloud} here is different from the hundreds of meters and kilometers usually used for PMS OAP averaging. Gultepe et al. (2000) studied the ice particle concentration averaged over the distance of 3 km and its dependence upon temperature for these four projects in some detail. For such small averaging scales (10^{-1} to 10^0km), the concentration may peak up to 10^2L^{-1} or even 10^3L^{-1} at some points inside a cloud. Gultepe and Isaac (1998) discuss the importance of averaging scales for determining microphysical parameters. However, since concentrations in this study are averaged over the meso- or synoptic scale, the results may be most useful for interpretation larger scales associated with satellite images and climate modeling.

The estimated average particle number concentrations N_{125} , N_{250} , and N_{500} , for sizes $D>125\mu\text{m}$, 250 μm and 500 μm , respectively, in different temperature intervals are shown in Tables 2-6. On average, the concentration N_{125} is approximately constant (about 3 to 4 L^{-1}) in the temperature interval $0^\circ\text{C}>T>-35^\circ\text{C}$. Below -35°C the concentration N_{125} rapidly decreases (Fig. 9). N_{250} stays nearly constant (about 1.5 L^{-1} -1.8 L^{-1}) for temperatures down to -30°C and then it decreases (Fig. 9). The concentration N_{500} has a maximum (about 1.2 L^{-1}) around -15°C , and decreases below this temperature (Fig. 9).

The estimated concentrations N_{125} , N_{250} , and N_{500} should be interpreted as the concentration of *ice* particles. The effect of supercooled drops (classified as “spheres”) in the worst case does not exceed 20% (Table 3) in the temperature interval $-10^\circ\text{C}<T<0^\circ\text{C}$. It is likely that a significant part of the particles recognized as “spheres” were frozen drops or compact irregulars. This reduces the fraction of supercooled drops. The maximum effect of supercooled drops on the concentration in the temperature interval $-45^\circ\text{C}<T<-10^\circ\text{C}$ is estimated as less than

7% (Tables 6). Taking into account that the probability of freezing rapidly increases with temperature decrease, the fraction of liquid droplets at $T < -10^{\circ}\text{C}$ can be estimated as a few percent or less.

6. DISCUSSION

(a) *Cloud top temperature versus measurement level temperature.*

It could be argued that the crystal habits should be related to the cloud top temperature rather than the measurement level temperature. However, most of the ice crystals observed occur at the smallest sizes, near $125\ \mu\text{m}$ for this study. These crystals will grow very rapidly – over a few hundred seconds – to this size. Consequently, during transport from cloud top or from near cloud base, the particles would either sublime to smaller sizes or grow to much larger sizes. For this reason, it makes most sense to use the measurement level temperature for the correlation. The fact that columnar and dendritic shapes in Fig. 6 peak near their expected formation temperatures determined from laboratory studies supports the use of the measurement level temperature.

(b) *Number of habit categories for particle classification.*

The number of categories in any automated processing technique should be a compromise between the potential of the probe to define the images (i.e. resolution, number of gray levels, occurrence of out-of-focus images, etc.) and the problem under solution. For example, for the calculation of the radiative properties of clouds, the role of pyramids and cups (C1a and C1b in the Magono-Lee classification) is negligible, since these type of ice particles rarely occur in the atmosphere. On the other hand the effect of columns and bullet rosettes on the radiative balance of the Earth may be significant because of their high frequency of occurrence in cirrus clouds.

Though some algorithms for habit classification use up to nine categories of cloud particles, in this study only four categories were used: spheres, irregulars, needles, and dendrites. This was done for the following reasons. First, these four categories cover the major ice particle habits in natural clouds: spherical, columnar, planar, and irregular. Some authors used rarely occurring categories like capped columns (Rahman et al. 1981) or hexagonal plates (Duroure 1982; Holroyd 1987; Garbric et al. 1995). Observations of ice particles at the ground level conducted by Zamorsky (1955) showed that the frequency of occurrence of plates and columns with plates is 2.8% and 2%, respectively. The analysis of high resolution CPI images of ice particles in Arctic clouds (Korolev et al. 1999) showed that pristine columns ($A/C > 1$), thick plates ($1 \geq A/C \geq 0.2$) and plates ($A/C < 0.2$) occur in the relative ratios 100:12:8 averaged over the temperature interval $-45^{\circ}\text{C} < T < 0^{\circ}\text{C}$. Hence, taking into account that the fraction of needles/columns is 7% (Table 6), the fraction of plates can be estimated as 0.6%. Therefore the effect of these categories was estimated as negligible. Observations of Zamorsky (1955) and Korolev et al. (1999) are consistent with a simple visual analysis of OAP-2DC data: plates and capped columns occur rarely in OAP-2DC imagery. Two frequently occurring habit categories, needles and columns, were merged into one category since the coarse resolution of the probe ($25\ \mu\text{m}$) does not make it possible to resolve these two habits for the majority of cases.

Adding more categories for the current algorithm would reduce its performance. The currently used categories have distributions of ratios that are well separated. Additional habit categories may have geometrical ratio distributions close to existing distributions. This, together with the inherent errors of statistical sampling, will lead to an increased error in classifying habits.

(c) *The effect of particle orientation on habit statistics*

The illuminating laser beam of the OAP-2DC installed on the NRC Convair-580 was purposely oriented vertically. Since an ice particle with the Reynolds number $Re > 10$ (List and Schemenauer 1971) falls with its largest cross section plane oriented horizontally, it is expected that the OAP-2DC measures the largest projection of the particle, i. e. when the particle image exhibits its best orientation for habit classification. From laboratory studies (List and Schemenauer 1971; Hallett et al. 2000), columns fall with their c -axis horizontal, while for plates and dendrites the c -axis is vertical. As mentioned in Section 3c, planar ice particles, like plates and dendrites, may give a rectangular projection, which may be recognized as a needle or column. In the case of aircraft measurements this may occur as the ice particle changes its natural orientation due to wind shear caused by the effect of the aircraft and the local flow around the instrument. If this were the case, we would observe on a regular basis in zones of dendrites a constant fraction of images classified as "needles" due to re-orientation of dendrites. Similarly in zones of needles, a certain fraction of circular images would be observed all the time. However, such a co-existence of shapes is not observed (e.g. see Fig. 5c,d), and the effect of re-orientation of planar and columnar ice particles on the habit statistics is estimated as no larger than a few percent.

(d) *Dependence of habit frequency of occurrence on particle size*

As discussed in section 4, the fraction of particle habits is not evenly distributed in different size intervals and it is a function of particle size. This observation is in qualitative agreement with the laboratory observation of dendritic growth (Hallett and Mason 1958). The growth of plates along the a -axis is changed to dendritic growth when the terminal fall velocity exceeds a certain threshold ($Re > 0.5$) (Alena et al. 1990). Since the terminal fall velocity is related to plate size, there is a threshold plate size for dendritic growth. For typical atmosphere conditions, it is about $200\mu\text{m}$. A particle starts to exhibit stellar or dendritic features only when it reaches some $400\text{--}600\mu\text{m}$ in size. This explains why in OAP imagery the frequency of occurrence of "complete" dendrites (with $D < 800\mu\text{m}$) is significantly less than that of "partial" dendrites.

(e) *Formation of irregularly shaped ice particles.*

The results of this study raise important questions: What is the mechanism for the formation of irregularly shaped ice particles? Why are habits of ice particles observed in natural clouds different from the habits observed in laboratory conditions? There are several possible mechanisms for the formation of such ice particles discussed in literature: (i) freezing of droplets as polycrystals (Hallett 1964; Jiusto and Weickmann 1973); (ii) falling ice particles through layers with different conditions; (iii) riming; (iv) aggregation.

Small-scale vertical cycling motions ($10^1\text{--}10^2$ m) of cloud parcels may be another possible mechanism for irregular ice particle formation. Cycling turbulent motions would lead to cycling changes in supersaturation inside a turbulent parcel (Korolev 1995). Supersaturation is negative during descent and positive during ascent. The cycling supersaturation in turn would cause cyclic sublimation and growth of ice particles. Sublimation may result in numerous irregularities on the surface of the ice crystal resulting from bending of crystals at points of weakness in the ambient airflow. This effect is clearly shown in the laboratory studies of Dong et

al. (1994). Subsequent growth of these reoriented crystals in different directions from the mother-crystal provides a second mechanism for the formation of polycrystals. Local differences of vertical velocity also lead to differences in supersaturation to give different growth rates and dendrite form and axial symmetry (Knight and Hallett 1994).

(f) *Cellular structure of needles and dendrites zones*

As was mentioned in Section 4, needles and dendrites occur in cells with a characteristic horizontal scale of hundreds of meters to tens of kilometers and concentrations up to $10\ l^{-1}$ (Fig. 4). These cells are usually surrounded by regions of irregularly shaped particles. This observation raises a question: what conditions cause needles and dendrites to form in such localized zones? Laboratory studies (e.g. Nakaya 1954; Kobayashi 1957; Hallett and Mason 1958; Rottner and Vali 1974; Alena et al., 1990) showed that the major parameters governing ice crystal habit and internal structure are temperature and water vapor supersaturation, enhanced by fall velocity. It may be hypothesized that the cells of needles and dendrites are associated with zones of uniform supersaturation (Hallett et al. 2000). One source of supersaturation is a large-scale slow ascent; alternatively localized regions of higher stability may lead to supersaturation through a heat/vapor diffusion process. However this explanation raises another question: what is the mechanism of ice nucleation in the cells of dendrites and needles? Why does the fraction of the dendrites or needles reach 100% in a particular place while a few kilometers away the concentration of dendrites or needles is zero? Are needles and dendrites growing from existing irregularly shaped ice particles, falling from above, or does the nucleation of the needles and dendrites occur inside these cells? The dendritic and needle shape of ice particles in the cells indicate that the ice particles were nucleated and were growing as monocrystals. The mechanisms of ice multiplication due to particle fragmentation during evaporation (Dong et al 1994) or the Hallett-Mossop mechanism (Hallett and Mossop 1974) cannot explain the cellular structure of dendrites as riming and evaporation were not evident. Non-equilibrium interactions between particles of different sizes and in different stages of growth/melt/evaporation near the 0°C level, producing small single crystal nuclei remains a possible mechanism for further study.

(g) *Concentration*

The results obtained in Section 5 show that at cold temperatures ($-45^{\circ}\text{C} < T < -35^{\circ}\text{C}$), on average, the concentration of particles with $D < 250\ \mu\text{m}$ is about 70% of the total $> 125\ \mu\text{m}$. Large particles $D > 500\ \mu\text{m}$ occur rarely (less than 4% of particles $> 125\ \mu\text{m}$), and its fraction increases with temperature. No statistically significant maximum in concentration N_{125} was found on the mesoscale, like those observed by Hobbs et al (1980) in the temperature range -12°C to -16°C .

The constant concentration of ice crystals (N_{125} and N_{250}) with temperature ($T > -35^{\circ}\text{C}$) in the troposphere shown in Fig. 9 is very important result. Past works have suggested an increase in concentration with colder temperatures (e.g. Meyers et al., 1992). Gultepe et al., (2000) suggest that this lack of relationship also holds for smaller ice particles ($< 125\ \mu\text{m}$). No simple explanation for this observation is possible at this time. However, particle breakup, aggregation, ice multiplication (e.g. Hallett and Mossop, 1974) are temperature dependent processes and do not provide a solution. Ice multiplication due to particle breakup caused by evaporation or sublimation can occur at any temperature under non-steady conditions as ice particles fall from aloft into sub ice saturated regions, or by turbulent mixing with sub saturated air. However, the exact mechanism for why such a process would lead to the concentration of ice particles being independent of temperature remains unclear and requires further study.

Another surprising result is rather sharp decrease of N_{125} below -35°C . Small crystals below the $125\ \mu\text{m}$ resolution limit are a key to interpretation of the variations in concentration with temperature.

7. TOWARDS A PHYSICAL CLASSIFICATION OF PARTICLE SHAPE

The utility of morphological studies is that they may help develop techniques to predict ice crystal habit and concentration. The following considerations help in such predictions:

- (a) growth from a single crystal - such as a frozen droplet or secondary ice particle - leads to a single crystal with facets and habit dependent on temperature. The skeletal structure in specific directions depends on supersaturation, modified by fall velocity.
- (b) growth from a polycrystal - as a larger droplet frozen at high supercooling - leads to a number of individual crystals radiating from a central point as a spatial array, with crystal form depending on temperature and supersaturation (columns, bullet rosettes; needles; plates, dendrites). Crystal reorientation may occur in association with evaporation or crystal deformation without fracture, followed by regrowth in an updraft.
- (c) Subsequent growth at lower supersaturation, well below saturation with respect to water, depends on defect structure introduced at nucleation leading to bicrystals and alternative symmetry (trigonal growth) leading to high linear growth rates which may dominate the relative proportion of crystal shapes at larger sizes.

Concentration data can be interpreted in terms of the latter process when defect growth is initiated and continues throughout the growth phase of the crystal; the large crystal sizes will be dominated by such growth whereas smaller sizes of similar mass may be dominated by crystals defective in several directions.

Data on the concentration in Tables 2-6 and Fig. 9 can be interpreted not only in terms of primary/secondary nucleation but also in terms of the differential growth rate of defective crystals that lead to larger crystals dominating under specific nucleation conditions that lock in at lower supersaturations. The set of data from Table 4 shows a maximum in concentration N_{125} near $-30^{\circ}\text{C} < T < -25^{\circ}\text{C}$ suggesting a possible nucleation process near this temperature leading to larger crystals resulting from greater linear growth rates from preferred defect structure. Further interpretation requires analysis of the habits of smaller crystals that can be obtained by replicator and CPI probes and will be given in a subsequent paper. Such an approach leads to a physical interpretation of crystal morphology with the ability to predict ice particle habits and concentration under specific nucleation and growth conditions.

8. CONCLUSION

This study concentrates on particles $> 125\ \mu\text{m}$ in size. This size is determined by the ability to classify the shapes of particles measured by a PMS 2DC probe with a $25\ \mu\text{m}$ pixel resolution. Conclusions cannot be drawn about the shapes of smaller particles which might be very important for radiative calculations, especially in cirrus clouds. However, for some studies (e.g. remote sensing by radars) the shapes of the larger particles are more important. For precipitation growth calculations, it can also be argued that the shape of the larger particles is also more important. This study provides useful information on these ice particles.

In the frame of this study the following results were obtained:

- (a). A new algorithm for particle recognition was developed. One of the advantages of this algorithm is that it processes both "complete" and "partial" images. This makes it possible to increase the number of processed images and significantly improves the statistics as compared to previous algorithms.

- (b). The frequency of occurrence of four habit categories (irregulars, dendrites, needles and spheres) was found. The majority of ice particles ($D > 125 \mu\text{m}$) were found to have an irregular shape (84%).
- (c). The frequency of occurrence of ice particle habit was found to depend on particle size. The fraction of irregulars decreases with increasing in particle size in the temperature intervals $0^\circ\text{C} < T < -15^\circ\text{C}$ and $-35^\circ\text{C} < T < -45^\circ\text{C}$. In the temperature interval $-35^\circ\text{C} < T < -15^\circ\text{C}$, the fraction of irregulars stays approximately constant with size.
- (d). Ice particles observed in natural clouds frequently did not fit into the Magono-Lee diagram.
- (e). The concentration of ice particles larger $125 \mu\text{m}$ averaged over 10^2 - 10^3 km scale is approximately 2.5 - 3.7 l^{-1} and it does not depend significantly on temperature in the range $-35^\circ\text{C} < T < 0^\circ\text{C}$. The concentration of ice particles larger $500 \mu\text{m}$ decreases below -15°C .
- (g). Needles and dendrites were found to form in cells with a characteristic horizontal scale of hundreds of meters to tens of kilometers embedded in zones of irregularly shaped particles.

In order to understand the role of ice in weather and climate, it is useful to have a climatology of ice particles as a function of habit, size, concentration, and surface area. The simplicity of the climatology presented in this paper should not be overlooked as a modeling approach. In spite of the coarse resolution of the OAP-2DC probe, the statistics obtained regarding particle habits show the characteristic features of ice particles ($> 125 \text{ mm}$) in natural clouds. These results may be used to improve weather and climate models. Further improvement in classification of ice particle habits using probes with higher resolution would make it possible to distinguish more categories and accomplish a more detailed image analysis.

ACKNOWLEDGEMENTS

The Panel on Energy Research and Development provided financial support for BASE and FIRE.ACE. Additional support for the collection of the FIRE.ACE data was given by NASA. The National Search and Rescue Secretariat of Canada, Boeing Commercial Airplane Group, Transport Canada, and the Canadian Department of National Defense provided funding for the CFDE project. The aircraft data were obtained using the National Research Council of Canada Convair-580 and the scientific and technical efforts of many NRC and MSC staff. The authors are particularly grateful to S. G. Cober for his helpful comments related to the relationship of particle habit and particle size. The assistance of J. W. Strapp and S. G. Cober of MSC and D. L. Marcotte of NRC in conducting the field projects is gratefully acknowledged. J. Hallett was supported by grant ATM-9413437 and ATM-9900560 from Division of Physical Meteorology, National Science Foundation, Arlington VA and a grant from NASA NAG-1-20466. Special thanks to Laura Hinkelman of Department of Meteorology (PennState) for discussion and valuable comments.

REFERENCES

- Alena, T., Hallett, J. and Saunders, C. P. R. 1990 On the facet-skeletal of snow crystals: experiments in high and low gravity. *J. Crystal Growth*, **104**, 539-555
- Bentley, W. A. 1902 Studies among the snow crystals during the winter of 1901-2 with additional data collected during previous winters. *Month. Weath. Rev.*, 607-616
- Bentley, W. A. and Humphreys, W. J. 1931 *Snow Crystals*. McGraw, New York
- Descartes, R., 1902 *Œuvres*. Tome VI, Paris, L. Cerif.
- Dong, Y.Y. R. Orltay, G. and Hallett, J. 1994 Ice particle generation during evaporation. *J. Atmos. Res.*, **32**, 45-53
- Durore, C., 1982 Une nouvelle metode de traitement des images d'hydrometeores données par les sondes bidimensionnelles. *J. Rech. Atmos*, **6**, 71-84
- Durore, C., Larsen, H. R., Isaka, H. and Personne, P. 1995 2D image population analysis. *Atmos. Res.*, **34**, 195-205
- Fouilloux, A., Iaquina, J., Durore, C. and Albers, F. 1997 A statistical analysis for pattern recognition of small cloud particles sampled with a PMS OAP-2DC probe. *Annales Geophysicae*, **15**, 840-846
- Garbrick, D. Chandrasekar, V. and Xiao, R. 1995 Neural network based classification procedure for 2D-PMS ice crystal images. Conference on Cloud Physics, Dallas, January 15-20. American Meteorological Society, Boston, USA, 59-64
- Gultepe, I. and Isaac, G.A. 1998 Scale effects on the relationship between cloud droplet and aerosol number concentrations: Observations and models. *J. Climate*, **12**, 1268-1279
- Gultepe, I., Isaac, G. A. and Cober, S. G., Strapp, J. W. 2000 Ice crystal concentration versus temperature. *Submitted to J. Appl. Meteor.*
- Hallett, J. 1964 Experimental studies of the crystallization of supercooled water, *J. Atmos. Sci.*, **21**, 671-682
- Hallett, J. 1976 Measurements of size, concentration and structure of atmospheric particles by continues replicator. Final Report, Contract AFG-TR-76-1049, Airforce Geophysical Laboratory
- Hallett, J. and Mason, B. J. 1958 The influence of temperature and supersaturation on the habit of ice crystals grown from the vapor, *Proc. Roy. Soc.*, **A247**, 440 -453
- Hallett, J. and Mossop, S. C. 1974 Production of secondary particles during the riming process, *Nature*, **249**, 26 -28
- Hallett, J. Arnott, W. P. Bailey, M. P. and Hallett, J. T. 2000 Ice Crystals in Cirrus , in *Cirrus*, Oxford University Press, in press
- Heymsfield, A J. and Parrish, J. 1979a Technique employed in the processing of particle size spectra and state parameter data obtained with the T-28 aircraft platform. NCAR Technical Note: NCAR/TN-137+1A
- Heymsfield, A J. and Parrish, J. 1979b A computational technique for increasing the effective sampling volume of the PMS two-dimensional particle size spectrometer. *J. Appl. Meteor.*, **17**, 1566-1572
- Hobbs, P. 1974 *Ice Physics*. Oxford University Press
- Hobbs, P., Politovich, M. K. and Radke, L. F. 1980 The structures of summer convective clouds in Eastern Montana. I: Natural clouds. *J. Appl. Meteor.*, **19**, 645-663
- Holroyd, E.W. 1987 Some techniques and uses of 2DC habit classification for snow particles. *J. Atmos. Ocean. Tech.*, **4**, 498-511
- Hunter, H. E. Dyer, R. M. and Glass, M. 1984 A two-dimensional hydrometeor machine classifier derived from observed data. *J. Atmos. Ocean. Tech.*, **1**, 28-36

- Isaac, G. A. 1991 Microphysical characteristics of Canadian Atlantic storms. *Atmos. Res.*, **26**, 339-360
- Isaac, G. A. Cober, S. G. Korolev, A. V. Strapp, J. W. Tremblay, A. and Marcotte, D. L. 1998 Overview of the Canadian Freezing Drizzle Experiment I, II and III. Conference on Cloud Physics, Everett, August 17-21. American Meteorological Society, Boston, USA, 447-450
- Jiusto, J. E. and Weickmann, H. K. 1973 Types of snowfall, *Bull Amer. Met. Soc.*, **54**, 1148-1162.
- Keller, V. and Hallett, J. 1982 Influence of air velocity on the habit of ice crystal growth from the vapor. *J. Crystal Growth*, **60**, 91-106
- Knight, A. C. and Hallett, J. 1994 On the symmetry of snow dendrites, *J. Atmos. Res.*, **32**, 1-11
- Knollenberg, R. G. 1981 Techniques for probing cloud microstructure. In: *Clouds, their formation, Optical properties, and Effects*, P. V Hobbs, A. Deepak, Eds. Academic Press, New York
- Kobayashi, T. 1957 Experimental researches on the snow crystal habit and growth by means of a diffusion cloud chamber, *J. Meteor. Soc. Japan 75th Anniv. Vol.*, 38-44
- Korolev, A. V., 1995 The influence of supersaturation on droplet size spectra formation. *J. Atmos. Sci.*, **52**, 3620-3634
- Korolev, A. V. Strapp, J. W. and Isaac, G. A. 1998 Evaluation of accuracy of PMS Optical Array Probes. *J. Atmos. Ocean. Tech.*, **15**, 708-720
- Korolev, A. V. Isaac, G. A. and Hallett, J. 1999 Ice particle habits in Arctic clouds. *Geoph. Res. Lett.*, **26**, 1299-1302
- Korolev, A. V. and Sussman, B. 2000 A technique for habit classification of cloud particles. *J. Atmos. Ocean. Tech.* in press
- Lawson, P. R. 1997 Improved measurements in the mixed clouds and implication to cloud modeling, *WMO Workshop on Measurements of Cloud Properties for Forecast of Weather and Climate*, Mexico City, 23-27 June. World Meteorological Organization, Mexico City, Mexico 139-158
- Liou, K. N. and Takano, Y. 1994 Light scattered by non-spherical particles: Remote sensing and climate implications. *Atmos. Res.*, **31**, 271-298
- List, R. and Schemenauer, R. S. 1971 Freefall behavior of planar snow crystals, conical graupel, and small hail. *J. Atmos. Sci.*, **28**, 110-115
- Magono, C. and Lee, C. 1966 Meteorological classification of natural snow crystals, *J. Fac. Sci., Hokkaido Univ. Ser. VII*, **2**, 321-335
- Mason, B. J. 1994 The shapes of snow crystals – Fitness for purpose? *Q. J. R. Meteorol. Soc.*, **120**, 849-860
- Matrosov, S. Y. Reinking, R. F. Kropfli, R. A. and Bartam, B. W. 1996 Estimation of ice hydrometeor types and shapes from radar polarization measurements. *J. Atmos. Ocean. Tech.*, **13**, 85-96
- Meyers, M. P., P. J. DeMott, and W. R. Cotton, 1992: New primary ice-nucleation parameterizations in an explicit cloud model. *J. App. Meteor.*, **31**, 708-721
- Moss, S. J. Johnson, D. W. 1984 Aircraft measurements to validate and improve numerical model parameterization of ice to water ratios in clouds. *Atmos. Res.*, **34**, 1-25
- Nakaya, U. 1954 *Snow crystals, natural and artificial*. Harvard Univ. Press, Cambridge, MA
- Pruppacher, H. R. and Klett, J. D. 1997 *Microphysics of Clouds and Precipitation*. Kluwer Academic Publisher, London

- Rahman, M. M. Quincy, E. A. Jacquot, R. G. and Magee, M. J. 1981 Feature extraction and selection for pattern recognition of two-dimensional hydrometeor images. *J. Appl. Meteor.*, **20**, 521-535
- Rottner, D. and Vali, G. 1974 Snow crystal habit at small excesses of vapor density over ice saturation. *J. Atmos. Sci.*, **31**, 560-569
- Tou, J. T. and Gonzales, R. C. 1974 *Pattern recognition principles*. Addison-Wesley Publishing Company, London
- Zamorsky, A. D. 1955 *Ice in the atmosphere*. Akademia Nauk SSSR, Moscow
- Zhang, Y. Macke, A. and Albers, F. 1999 Effect of crystal size spectrum and crystal shape on stratiform cirrus radiative forcing. *Atmos. Res.*, **52**, 59-75

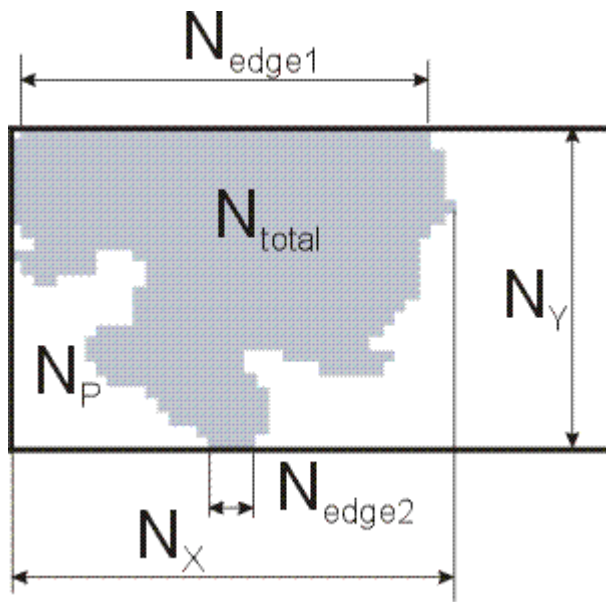


Figure 1. Simple measurable parameters used for image habit recognition

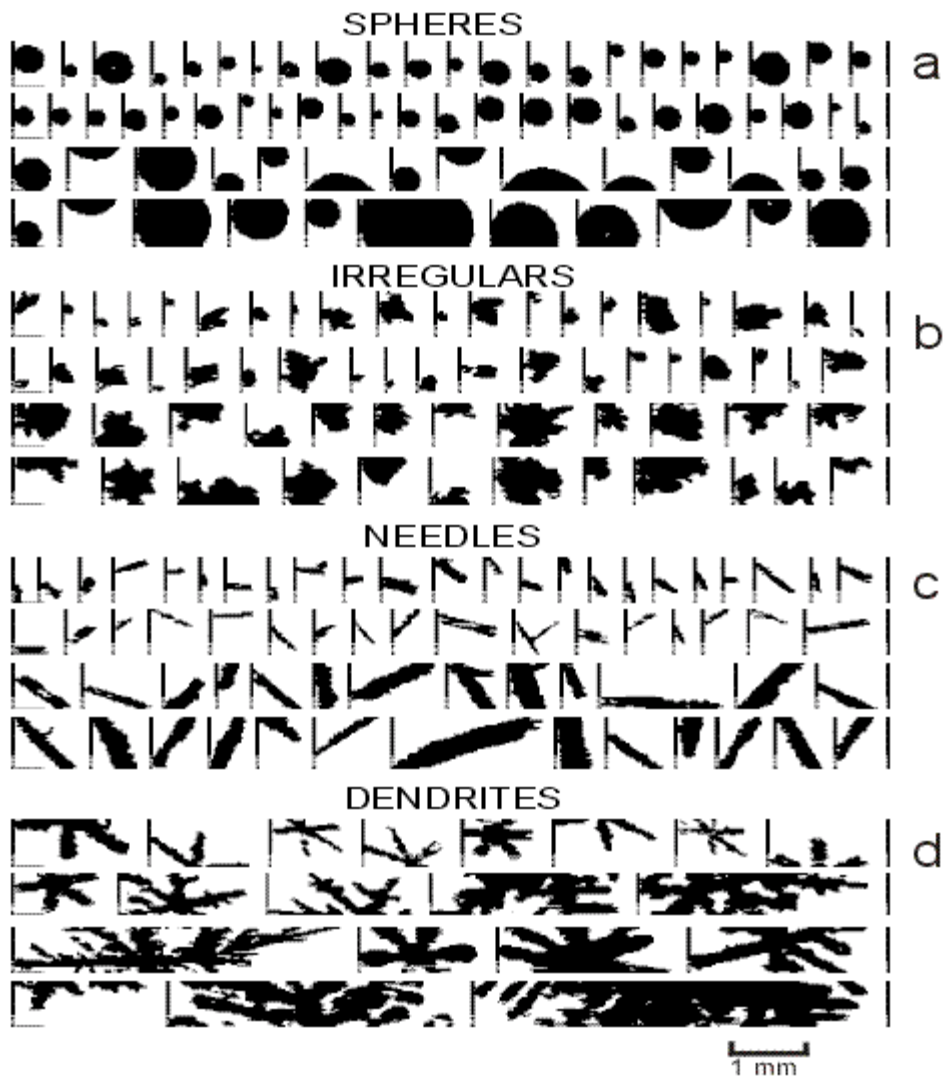


Figure 2. Classification of PMS OAP-2DC cloud particle images. (a) spheres; (b) irregulars; (c) needles and columns; (d) dendrites.

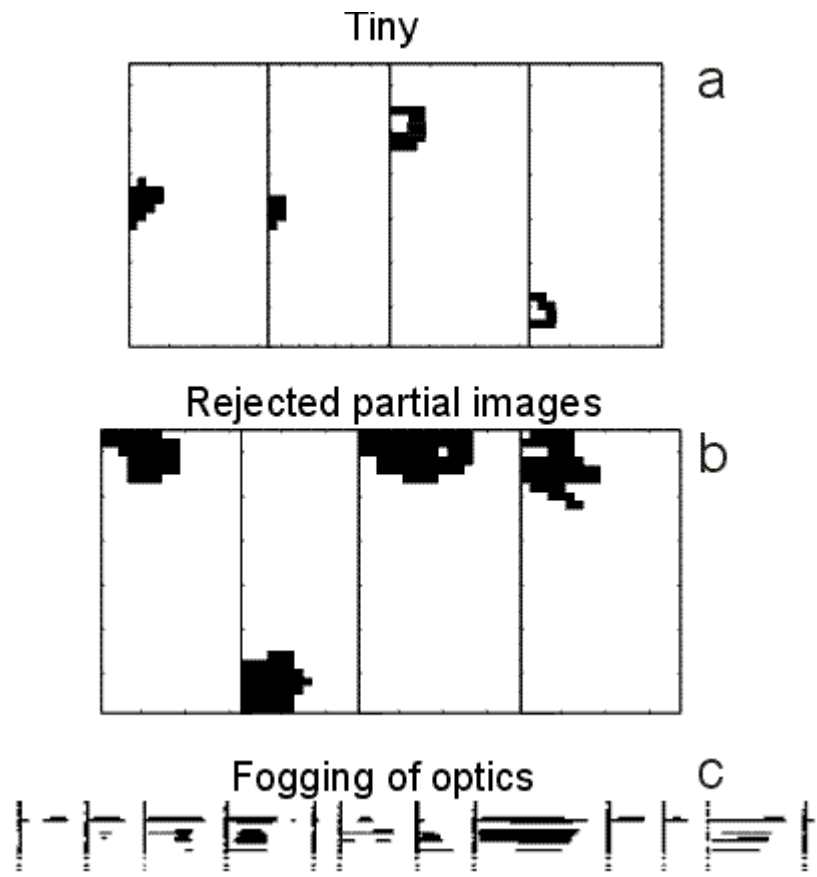


Figure 3. Examples of rejected OAP-2DC particle images. (a) “tiny”; (b) “rejected partials”; (c) degraded images due to optics fogging.

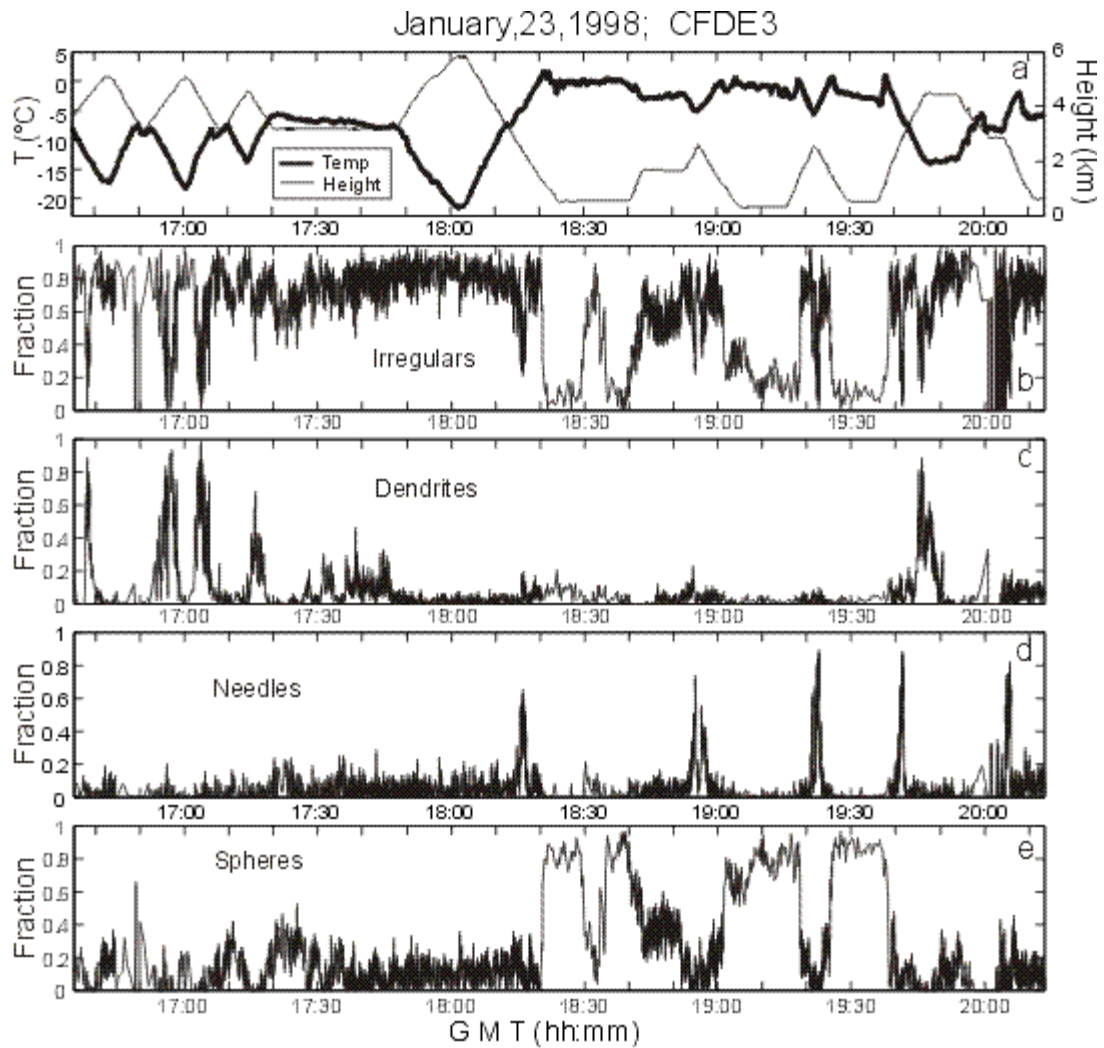


Figure 4. Changes of cloud particle habits during the flight on January 23, 1998 (CFDE III). (a) changes of temperature and altitude. Spatial changes of the fraction of (b) irregulars; (c) dendrites, (d) needles, (e) spheres

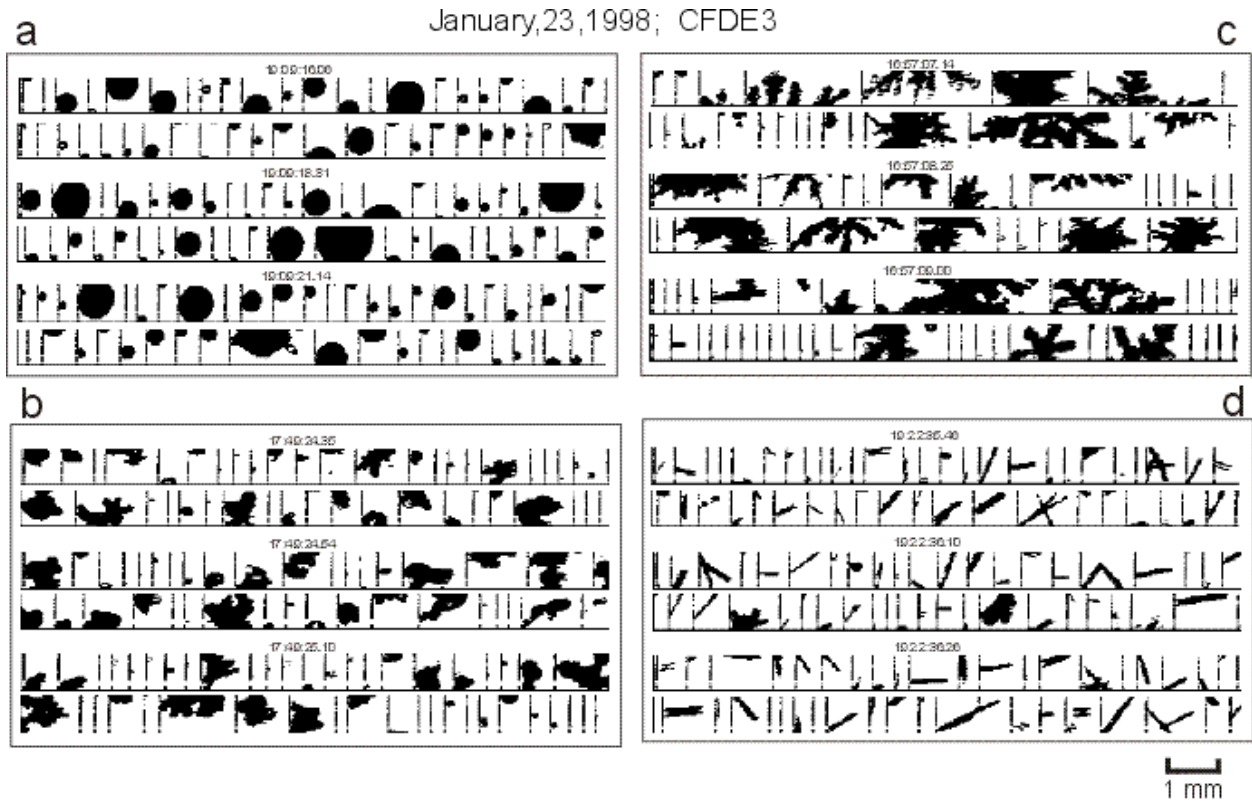


Figure 5. Samples of OAP-2DC images measured in zones of (a) spheres; (b) irregulars; (c) dendrites; (d) needles during the CFDE III flight on January 23, 1998 (Fig. 3). The measurement times are indicated at the top of each 2D buffer (32x1024 image slices). (time GMT).

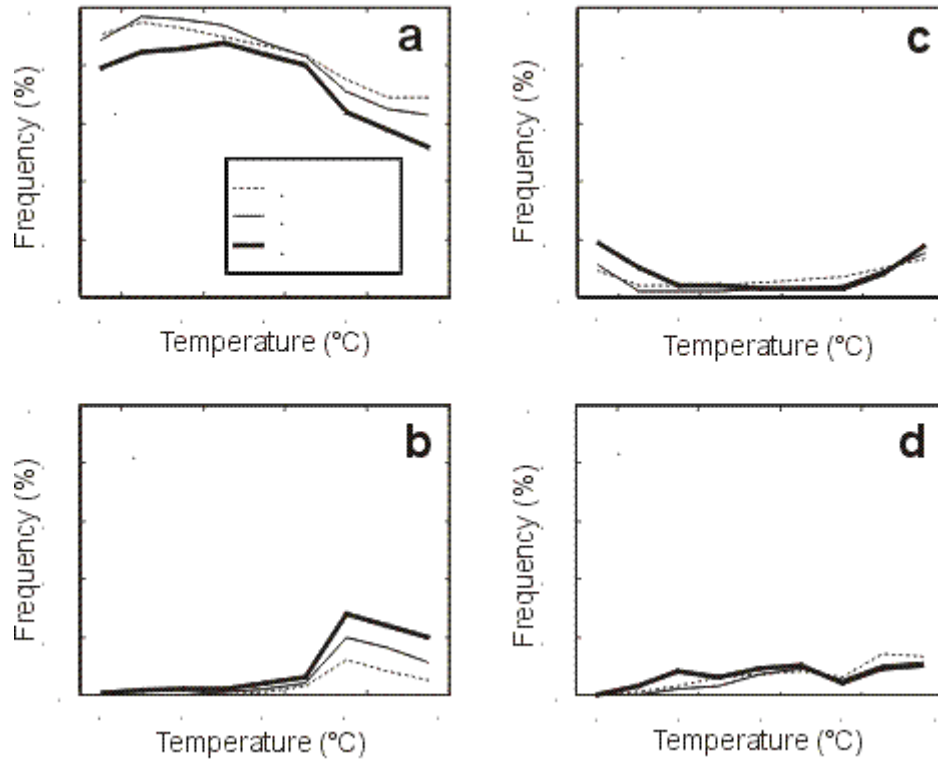


Figure 6. Dependence of the frequency of occurrence of habit categories versus temperature for different size intervals $D > 125 \mu\text{m}$; $D > 250 \mu\text{m}$; $D > 500 \mu\text{m}$. (a) irregulars, (b) dendrites (c) needles, (d) spheres.

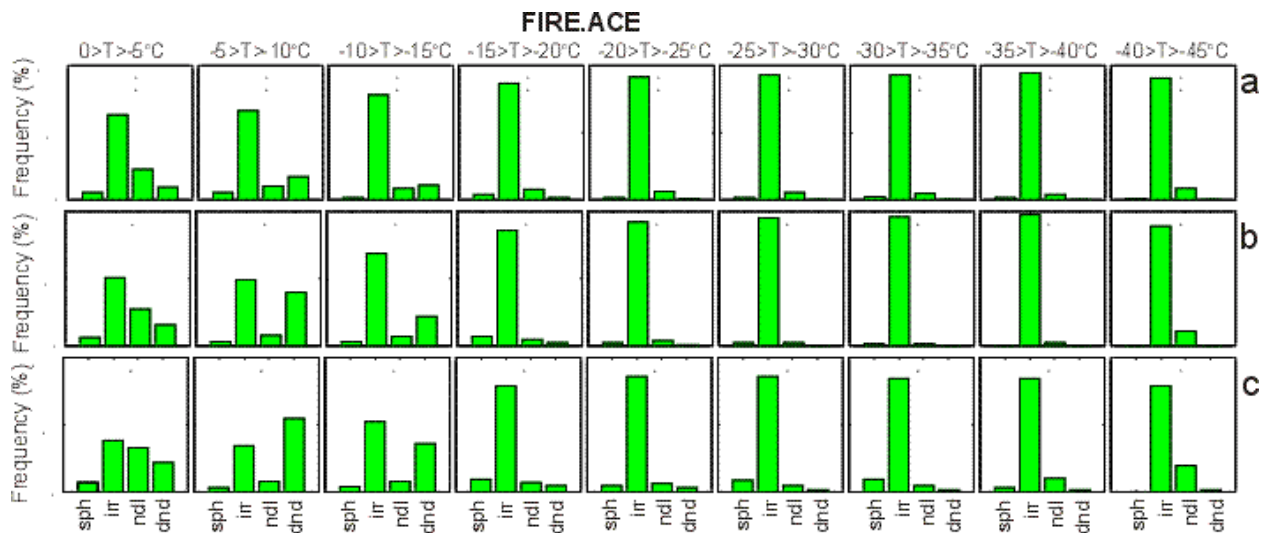


Figure 7. Frequency of occurrence of irregulars, dendrites, needles/columns and spheres versus temperature for particles larger 125µm (a); 250µm (b) and 500µm (c). The particle habits were derived from PMS OAP-2DC imagery measured during FIRE.ACE.

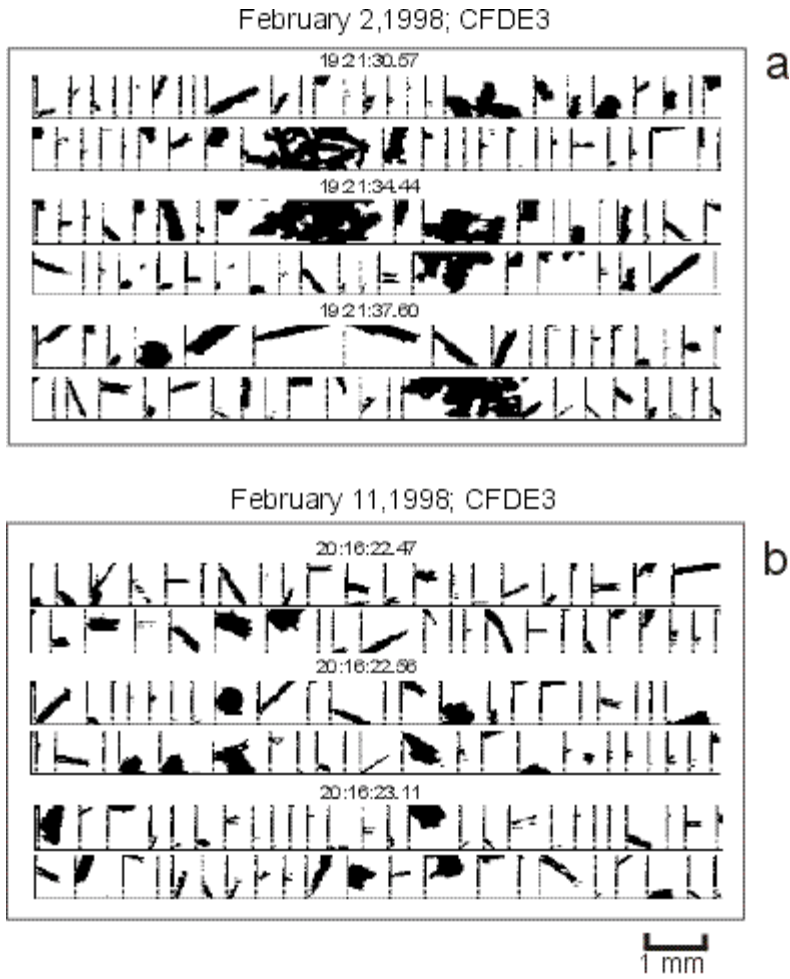


Figure 8. Example of mixtures of cloud particle having different habits. (a) mixture of irregulars, dendrites and needles. February 02, 1998; Nimbostratus, $H=1900\text{m}$; $T=-5^{\circ}\text{C}$; (b) mixture of needles and irregulars. February 11, 1998; Nimbostratus, $H=3200\text{m}$; $T=-6^{\circ}\text{C}$; (time GMT).

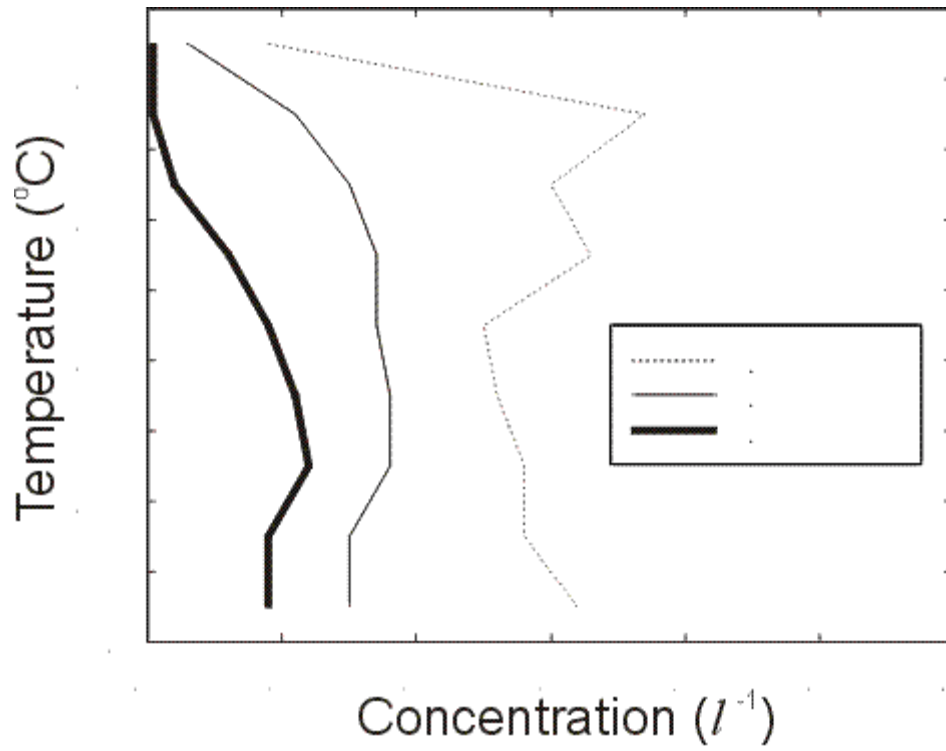


Figure 9. Averaged number concentration of cloud particles larger 125 μm 250 μm and 500 μm measured by the OAP-2DC during BASE, CFDE I, CFDE III, and FIRE.ACE.

TABLE 1. CHARACTERISTICS OF FLIGHT PROJECTS

Project name	Date	Flight region	Number of flights	In-cloud length (km)	path	Main air mass type
BASE	Sept.-Oct. 1994	57°N-74°N; 113°W-141°W	14	7,412		Arctic, Continental
CFDE I	March 1995	45°N-53°N; 54°W-63°W	8	6,518		Maritime
CFDE III	Dec.1997-Feb.1998	52°N-50°N; 71°W-83°W	26	19,764		Continental
FIRE.ACE	April 1998	68°N-76°N; 133°W-167°W	12	4,082		Arctic

TABLE 2. BASE, CANADIAN ARCTIC, SEPTEMBER-OCTOBER, 1994

Temperature	Fraction of spheres (%)			Fraction of irregulars (%)			Fraction of needle/columns (%)			Fraction of dendrites (%)			Number of images			Cloud length (km)	Particle concentration (l^{-1})		
	125 μ m	250 μ m	500 μ m	125 μ m	250 μ m	500 μ m	125 μ m	250 μ m	500 μ m	125 μ m	250 μ m	500 μ m	125 μ m	250 μ m	500 μ m		125 μ m	250 μ m	500 μ m
0>T>-5°C	4	4	4	70	65	57	14	14	12	11	17	27	138580	91280	60235	1328	2.1	1.4	0.9
-5>T>-10°C	8	6	4	68	60	52	7	5	4	17	29	39	132032	85188	60262	1670	1.6	1	0.7
-10>T>-15°C	3	2	2	69	61	55	7	5	4	21	32	40	88411	62918	48925	965	1.8	1.3	1
-15>T>-20°C	6	7	7	84	83	81	6	5	5	4	5	7	51132	37166	25992	638	1.6	1.2	0.8
-20>T>-25°C	7	8	9	88	89	86	4	3	4	0	1	1	72269	50862	28860	765	1.9	1.3	0.8
-25>T>-30°C	8	2	4	88	94	88	4	3	5	0	0	2	201151	108302	32482	1503	2.7	1.4	0.4
-30>T>-35°C	9	2	4	88	96	92	3	2	3	0	0	1	17606	7851	2153	186	1.9	0.8	0.2
-35>T>-40°C	2	0	0	95	94	0	3	6	0	0	0	0	2050	154	0	32	1.3	0.1	0
-40>T>-45°C	1	0	0	93	93	0	6	7	0	0	0	0	2519	966	0	42	1.2	0.5	0
0>T>-45°C	6	4	5	82	82	73	6	6	5	6	9	17	705750	444687	258909	7127	2	1.2	0.7

TABLE 3. CFDE I, NEWFOUNDLAND, MARCH, 1995

Temperature	Fraction of spheres (%)			Fraction of irregulars (%)			Fraction of needle/columns (%)			Fraction of dendrites (%)			Number of images			Cloud length (km)	Particle concentration (I^{-1})		
	125 μm	250 μm	500 μm	125 μm	250 μm	500 μm	125 μm	250 μm	500 μm	125 μm	250 μm	500 μm	125 μm	250 μm	500 μm		125 μm	250 μm	500 μm
0>T>-5°C	14	8	8	67	62	47	14	21	27	4	9	18	544517	253930	140286	2564	4.2	2	1.1
-5>T>-10°C	20	10	6	66	68	63	8	9	9	7	13	22	355085	163539	95361	1356	5.2	2.4	1.4
-10>T>-15°C	11	7	4	68	66	63	8	6	6	13	20	27	111281	74928	54668	817	2.7	1.8	1.3
-15>T>-20°C	7	8	7	86	86	87	4	3	2	2	3	4	23831	17810	11835	341	1.4	1	0.7
-20>T>-25°C	5	4	4	88	90	90	4	2	1	3	4	5	31724	23578	17327	456	1.4	1	0.8
-25>T>-30°C	4	4	4	91	93	93	4	2	1	1	2	2	49796	35270	23213	194	5.1	3.6	2.4
-30>T>-35°C	5	0	0	93	98	0	2	2	0	0	0	0	2464	337	0	23	2.1	0.3	0
0>T>-35°C	10	6	5	80	80	74	6	6	8	4	7	13	1118698	569392	342690	5754	3.9	2	1.2

TABLE 4. CFDE III, GREAT LAKES, DECEMBER, 1997-FEBRUARY, 1998

Temperature	Fraction of spheres (%)			Fraction of irregulars (%)			Fraction of needle/columns (%)			Fraction of dendrites (%)			Number of images			Cloud length (km)	Particle concentration (I^{-1})		
	125 μm	250 μm	500 μm	125 μm	250 μm	500 μm	125 μm	250 μm	500 μm	125 μm	250 μm	500 μm	125 μm	250 μm	500 μm		125 μm	250 μm	500 μm
0>T>-5°C	14	13	12	70	64	53	11	12	15	5	11	20	973382	457001	250036	6599	3	1.4	0.8
-5>T>-10°C	12	11	12	70	64	58	11	11	10	6	13	20	726503	381649	237388	5283	2.8	1.4	0.9
-10>T>-15°C	6	5	5	77	74	67	6	3	3	11	18	26	531292	342638	228447	3282	3.2	2.1	1.4
-15>T>-20°C	9	10	11	83	83	80	5	3	3	3	4	7	374061	259320	168104	1950	3.8	2.7	1.7
-20>T>-25°C	10	10	12	84	86	82	4	2	2	1	2	4	142425	99383	58550	835	3.4	2.4	1.4
-25>T>-30°C	6	5	9	91	93	88	3	2	2	0	0	2	94783	50562	16564	347	5.5	2.9	1
-30>T>-35°C	1	0	0	96	98	0	3	2	0	0	0	0	1739	637	0	13	2.7	1	0
0>T>-35°C	8	8	10	82	80	71	6	5	6	4	7	13	2844185	1591190	959089	18309	3.1	1.7	1

TABLE 5. FIRE.ACE, Canadian and US Arctic, April, 1998

Temperature	Fraction of spheres (%)			Fraction of irregulars (%)			Fraction of needle/columns (%)			Fraction of dendrites (%)			Number of images			Cloud length (km)	Particle concentration (I^{-1})		
	125 μm	250 μm	500 μm	125 μm	250 μm	500 μm	125 μm	250 μm	500 μm	125 μm	250 μm	500 μm	125 μm	250 μm	500 μm		125 μm	250 μm	500 μm
0>T>-5°C	5	6	7	64	51	38	22	27	33	9	16	22	8121	5385	3620	76	2.1	1.4	1
-5>T>-10°C	6	3	3	67	50	34	10	8	7	17	40	55	23429	11496	7625	372	1.3	0.6	0.4
-10>T>-15°C	2	3	4	78	68	52	9	7	8	11	22	36	42923	24101	13502	471	1.8	1	0.6
-15>T>-20°C	4	7	9	86	86	80	8	5	7	1	2	5	85013	49073	22729	1104	1.5	0.9	0.4
-20>T>-25°C	2	2	5	93	92	86	6	4	6	0	1	3	62313	31457	10518	404	3.1	1.6	0.5
-25>T>-30°C	2	2	8	93	96	87	5	2	5	0	0	1	81583	27879	5501	531	3.1	1.1	0.2
-30>T>-35°C	2	2	9	93	96	85	4	2	5	0	0	1	97168	48762	6217	568	3.4	1.7	0.2
-35>T>-40°C	1	0	3	95	98	86	4	2	10	0	0	1	94355	29225	1115	487	3.9	1.2	0.05
-40>T>-45°C	0	0	0	91	89	80	9	11	19	0	0	1	28806	10036	1327	637	0.9	0.3	0.04
0>T>-45°C	3	3	5	84	80	70	8	8	11	4	9	14	523711	237414	72154	4650	2.3	1	0.3

TABLE 6. SUMMARY OF BASE, CFDE I, CFDE III AND FIRE.ACE

Temperature	Fraction of spheres (%)			Fraction of irregulars (%)			Fraction of needle/columns (%)			Fraction of dendrites (%)			Number of images			Cloud length (km)	Particle concentration (I^{-1})		
	125 μm	250 μm	500 μm	125 μm	250 μm	500 μm	125 μm	250 μm	500 μm	125 μm	250 μm	500 μm	125 μm	250 μm	500 μm		125 μm	250 μm	500 μm
0>T>-5°C	13	11	10	69	63	52	13	15	18	5	11	20	1664600	807596	454177	10567	3.2	1.5	0.9
-5>T>-10°C	14	10	9	69	65	58	10	9	8	8	16	24	1237049	641872	400636	8681	2.8	1.5	0.9
-10>T>-15°C	6	5	4	75	71	64	7	4	3	12	20	28	773907	504585	345542	5536	2.8	1.8	1.2
-15>T>-20°C	8	9	10	84	83	80	6	3	3	3	4	6	534037	363369	228660	4034	2.6	1.8	1.1
-20>T>-25°C	7	7	9	87	88	84	5	3	3	1	2	4	308731	205280	115255	2460	2.5	1.7	0.9
-25>T>-30°C	6	3	6	90	94	88	4	2	4	0	1	2	427313	222013	77760	2575	3.3	1.7	0.6
-30>T>-35°C	3	2	8	93	96	86	4	2	4	0	0	2	118977	57587	8370	790	3	1.5	0.2
-35>T>-40°C	1	0	3	95	97	85	4	2	10	0	0	2	96405	29379	1115	519	3.7	1.1	0.04
-40>T>-45°C	0	0	0	91	89	80	9	11	19	0	0	1	31325	11002	1327	679	0.9	0.3	0.04
0>T>-45°C	7	5	6	84	83	76	6	6	8	3	6	10	5192344	2842683	1632842	35840	2.9	1.6	0.9